Microstructural Characterization of Injection-Molded Articles

MUSA R. KAMAL* and FRANCIS H. MOY,† *Department of Chemical Engineering, McGill University, Montreal, Canada H3A 2A7*

Synopsis

The techniques of density, X-ray diffraction, and infrared dichroism measurements were employed to study anisotropic behavior, as a result of processing, in injection-molded parts. Data pertaining to the distributions of crystallinity and orientation indicated that significant changes occur at or near the surface of the molding. Generally, maximum density (crystallinity) is observed in the core of the molding and near the gate, while minimum density (crystallinity) is observed near the surface. X-ray diffraction suggests a complex pattern of orientation for the three crystallographic axes. The crystallographic a-axis tends to be oriented in the flow direction as indicated by both X-ray diffraction and infrared dichroism measurements. Generally, raising the molding temperature has only marginal influence on crystallinity and orientation. However, the two resins included in the study exhibited substantial differences in the distribution of these properties. The distributions of crystallinity and orientation are attributable to the complex interactions between resin properties and process conditions.

INTRODUCTION

The quality of injection-molded articles is dictated by the properties of the resin and by the thermomechanical history experienced by the material during plastication and the high-speed injection of the melt into, quite often, a mold of complex geometry. For crystalline polymers, the interactions between the molten polymer and the thermal and mechanical conditions that exist in the mold cavity during the filling, packing, and cooling stages of the molding cycle influence the development of microstructure in the molded part. The microstructure, in turn, significantly affects the end-use properties of the molded article.

In recent published work in the area of thermoplastic injection molding, much of the effort has been directed to the modeling of the process, in order to shed some light on the thermomechanical history of the material during processing.[1–7] Other work has concentrated on the study of the morphology and orientation in injection molded parts.[8–22] Earlier work has concentrated on the measurement of internal (frozen-in) stresses in thermoplastic moldings mainly by means of polarizing optics such as birefringence[19–21] and analysis of X-ray scattering[12,13] or, indirectly, by measuring thermal shrinkage[15] and by determination of mechanical anistropy.[18]

Generally, work relating to the study of the microstructure of injection-molded partially crystalline polymers has tended to be fragmented and qualitative in nature. A variety of techniques have been employed to elucidate the nature of

* To whom all correspondence should be addressed.

† Present Address: Technical Center, Union Carbide of Canada, P.O. Box 600, Pointe-aux-Trembles, Quebec, Canada H1B 5K8.

Journal of Applied Polymer Science, Vol. 28, 1787–1804 (1983)
 CCC 0021-8995/83/051787-18$02.80

morphology and orientation and their distributions in these systems. These techniques indicate a complex skin-core structure with continuous variation of morphology and orientation throughout the molding. However, little has been done to integrate the results of various experimental techniques or to employ quantitative methods to relate results from various techniques to each other and to the ultimate properties of the moldings.

The present paper is part of a series,[4,5,17,22,23,25–29,46] which attempts to fill some of the void in the fundamental understanding of the injection molding process and related products. In the present work, data are reported regarding the detailed characterization of the microstructure of injection-molded polyethylene samples utilizing the techniques of density, X-ray, and infrared dichroism measurements. Other work has indicated that the optical and mechanical properties of injection molding parts may be estimated with reasonable accuracy from a knowledge of the distributions of crystallinity and orientation functions in the molding.[23] Therefore, microstructure, in the present context, is defined to reflect these distributions. Comparisons are made between crystallinity and orientation distributions employing two typical polyethylene molding resins. The effects of changes in molding temperature on microstructure are also considered.

EXPERIMENTAL

Preparation of Moldings

Two injection molding polyethylene resins (designated EX1 and EX2) were used in the study. The physical properties of the two materials are shown in

TABLE I
Physical Properties of Materials[a]

Physical properties	Resin material EX1	Resin material EX2	Source[b]
$\overline{M}_W$ (g/mol)	8.92×10^4	7.45×10^4	(1)
$\overline{M}_N$	1.75×10^4	2.23×10^4	(1)
$\overline{M}_W/\overline{M}_N$	5.09	3.33	(1)
Density (g/cm^3)	0.959	0.962	(1)
Melt index (g/10 min)	8.07	7.40	(1)
Melting range (°C)	113–146°C	113–146°C	(2)
Average specific heat [cal/g · °C)]			(3)
C_p solid	0.569	0.607	
C_p melt	0.589	0.587	
Average thermal conductivity (cal/cm · °C · s)			(3)
k_s solid	8.64×10^4	8.24×10^4	
k_m melt	6.24×10^4	6.25×10^4	
Average thermal diffusivity (cm^2/s)			(3)
α_s solid	20.6×10^4	18.9×10^4	
α_m melt	12.7×10^4	12.9×10^4	
Power law index n	0.800	0.822	(2)
$\Delta E/R$ (1/°K)	2338	2167.4	
A (g/cm/s^{n-2})	92.76	139.9	

[a] Note: $\eta_T = A \exp(E/RT)\dot{\gamma}_T^{n-1}$, where η_T is in poise, $\dot{\gamma}$ in s^{-1}, and T in °K.

[b] Sources: (1) DuPont of Canada Ltd; (2) Ref. 2; (3) Measurements made in this laboratory, not reported elsewhere.

Table I. It is known that resin EX1 includes species that might serve as heterogeneous nucleating agents, while such species are not present in EX2. Moldings were obtained employing a melt temperature of 176°C and a mold temperature of 35°C. Moldings were also obtained for resin EX2, employing a melt temperature of 205.9°C.

A reciprocating screw $2\frac{1}{3}$ oz Metalmec injection molding machine was used in conjunction with a center-gated mold cavity with dimensions: 12.7 cm × 6.35 cm × 3.18 mm. The gate width was 5.3 mm.

Microstructure Characterization

Long rectangular pieces (4.0 cm × 4 mm) were cut from the different moldings at various positions, as indicated in Figure 1. These samples were located at 2.0 cm, 6.0 cm, and 10.0 cm from the gate. Samples were also cut from the off-center positions. Thin sections of 40 μm thickness were sliced from the rectangular pieces, using a large Reichert microtome. The long thin microtomed sections were further cut into two sections, approximately (6 mm × 4 mm) and (4 mm × 4 mm), respectively. The longer microtomed sections (6 mm × 4 mm) were used for birefringence, wide-angle X-ray diffraction, and infrared dichroism measurements. The shorter sections (4 mm × 4 mm) were used for density measurements.

Distilled water and isopropanol were used to prepare a density gradient column which covered the range of 0.925–0.965 g/cc at 23°C.

The crystalline characteristics of the specimen were determined employing wide-angle X-ray measurements. The sections from the molding were irradiated with Ni-filtered CuK_2 radiation in a plane normal to the xy-plane of the specimen. The wide-angle X-ray diffraction patterns were recorded on photographic film. The voltage and current were 40 kV and 20 mA, respectively. The sample-to-film distance was 4.22 cm. The azimuthal intensity distributions of the (110), (200), and (020) reflections were determined from 0° to 90° in increments of 3°. The azimuthal intensity distributions were measured using a Joyce-Loebl Automatic Recording Microdensitometer Model MK III C.S.

Dichroic measurements corresponding to both the 720 cm^{-1} and 730 cm^{-1} absorption peaks were made on a Perkin-Elmer infrared grating spectrophotometer, Model 467, with the additional attachments of a sample space wire grid polarizer, a 4× beam condenser, and a demountable micro cell mount.

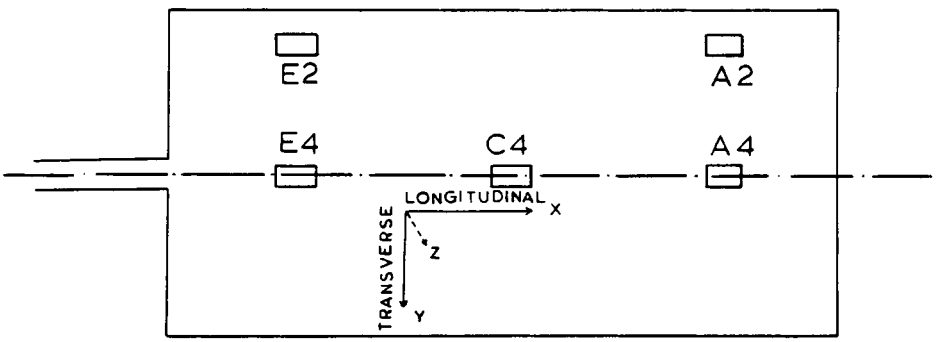

Fig. 1. Designated positions for microstructural studies in the depth direction of the moldings.

RESULTS AND DISCUSSION

Density Measurements

The crystalline volume fraction (X_c) is expressed as

$$X_c = \frac{(\rho_s - \rho_{am})}{(\rho_c - \rho_{am})} \quad (1)$$

where ρ_{am} is the density of the completely amorphous phase.[24] For polyethylene, ρ_{am} is taken to be 0.856 g/cc.[24] ρ_c is the density of the completely crystalline phase, and it is computed from unit cell dimensions to be 1.001 g/cc.[24] ρ_s is the measured sample density (g/cc).

The variation of polyethylene density (crystallinity) is an indication of the crystallization phenomena occurring during the injection molding process.[25] The variations of the density and volume fraction crystallinity as a function of the distance from the surface for the two resins at the indicated locations along the molding are shown in Figures 2 and 3. For the purpose of clarity, the results of the two off-center positions located near the gate and far from the gate are plotted together, but separately from the center line positions.

Generally, the density (crystallinity) increases monotonically, from a minimum value near the surface to a maximum towards the core region of the molding.

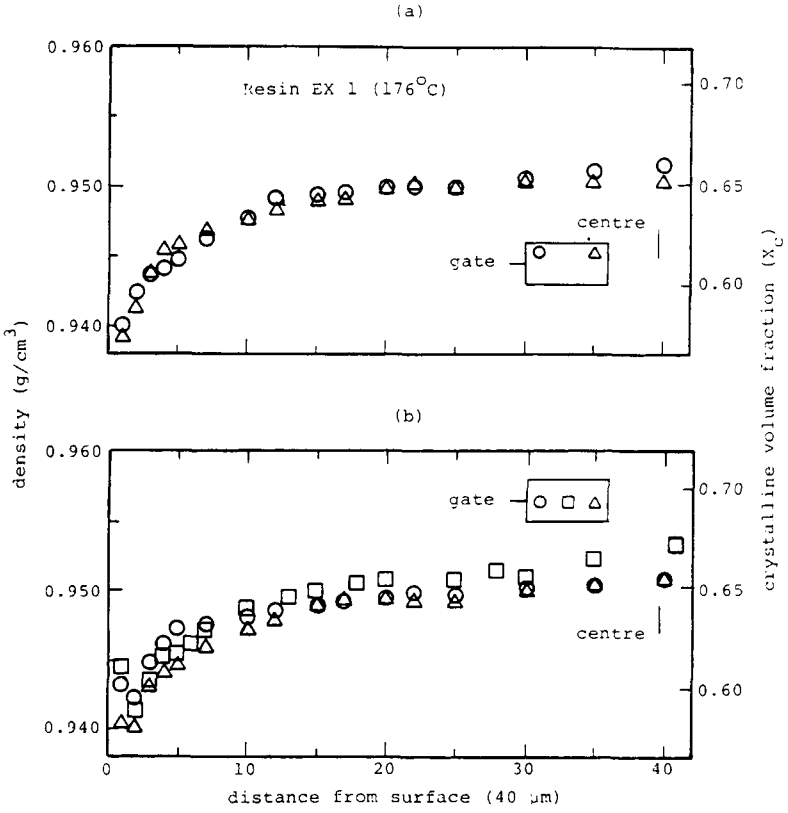

Fig. 2. Variation of density (crystallinity) in the depth direction.

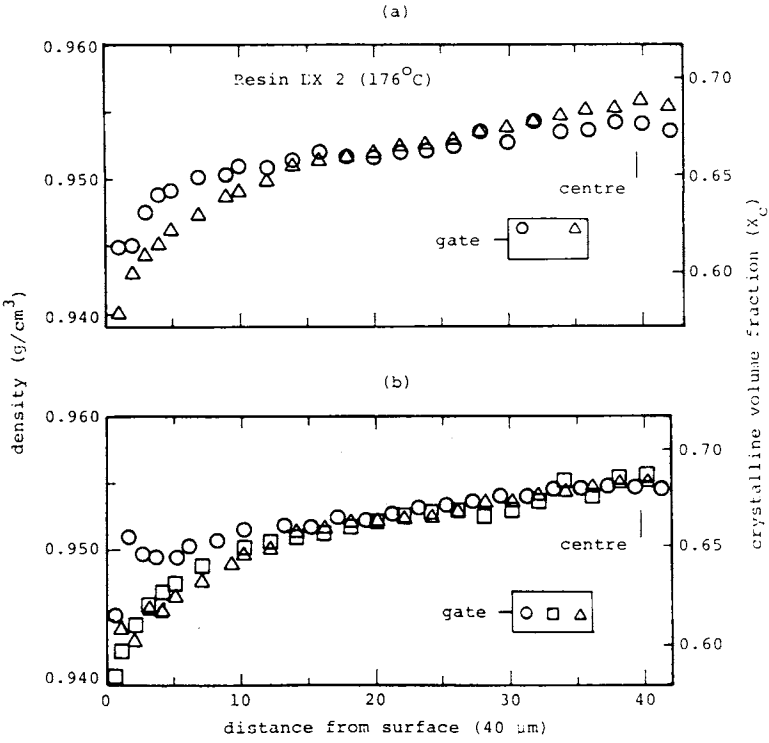

Fig. 3. Variation of density (crystallinity) in the depth direction.

Several workers[25,26] have reported similar variations in the distribution of density in the depth direction of the molding. The lower crystallinity near the surface of the molding is attributed to the rapid cooling of the melt near the mold surface, which reduces the extent of crystallization. Furthermore, the rapid cooling that melt elements experience near the cold mold surface causes the melt to incorporate more free volume than in the case of slow cooling. The higher densities observed towards the core of the molding are due to the lower thermal gradients and hence lower cooling rates, which enhance the growth of spherulites in this region.

Generally, the overall density is observed to be highest for the location near the gate and lowest for the location furthest from the gate. This behavior is attributed to the longer cooling times and higher packing pressures that prevail near the gate.[24,26] The above gate effects are observed mainly for material near the surface of the moldings.

For the off-center positions located both near the gate and far from the gate, there appears to be very little difference in the density distributions observed, as shown in Figures 2(a), 3(a), and 4(a). However, Figure 3(a) tends to show a difference between the two off-center locations for resin EX2 molded at a melt temperature of 176°C. The difference may be attributed to the slightly longer cooling times and higher packing pressures in the region located near the gate, as mentioned earlier. Although Figure 2(a) and 4(a) do not exhibit as marked a difference, a similar tendency appears to be evident.

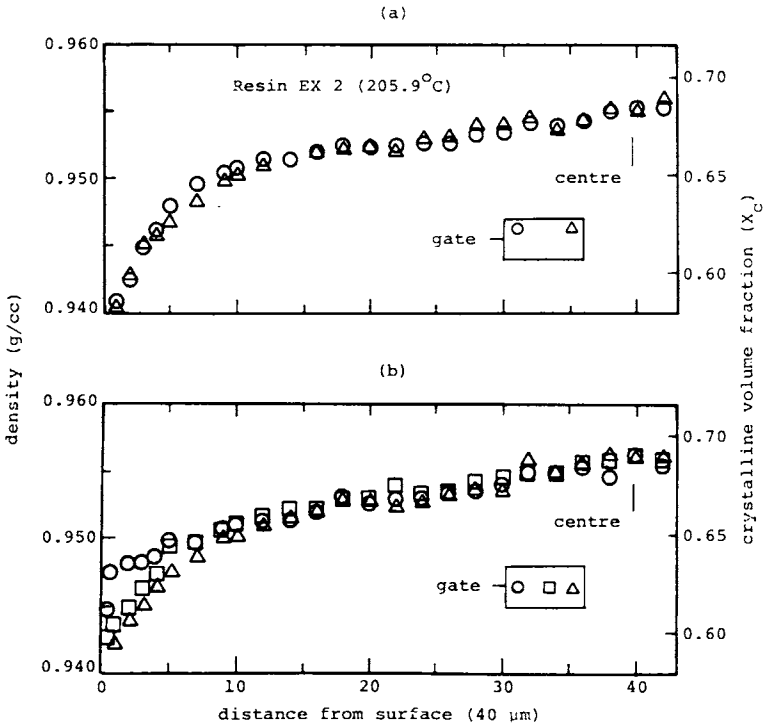

Fig. 4. Variation of density (crystallinity) in the depth direction.

Generally, resin EX2 tends to exhibit higher densities (crystallinities) throughout the molded part than resin EX1. This is due, in part, to the fact that resin EX2 has a higher solid density to begin with.[27,28] Furthermore, resin EX2 probably experiences lower effective cooling rates than resin EX1 since the former exhibits both a lower crystallization temperature, as shown by previous P-V-T and DSC data,[28,29] and lower thermal diffusivity[30].

At the high melt temperature, as shown in Figures 4(a) and 4(b), the relative density distributions are similar to those observed for the two resins molded at the lower melt temperature. Generally, increasing the injection melt temperature tends to marginally increase the density (crystallinity) throughout the molded part. This is attributed to the generally longer cooling times associated with the higher melt temperature[25] and the resulting lower effective cooling rates due to the balance of the prevailing thermal properties of the system.[30]

X-Ray Measurements

The crystalline contribution to the total orientation, for example as measured by birefringence, may be completely described in terms of the orientation functions defined as[31,32]

$$f_a = (3\,\overline{\cos^2\alpha} - 1)/2 \tag{2a}$$

and

$$f_b = (3\,\overline{\cos^2\beta} - 1)/2 \tag{2b}$$

TABLE II
Spacing of Reflected Planes[a]

Diameter of ring D (cm)	$2\theta = \tan^{-1}(D/2L)$	$d_{hkl} = \lambda/2 \sin\theta$(Å)[a]	Miller indices (hkl)
3.35	21° 38′	4.10 (4.102)	(110)
3.78	24° 6′	3.69 (3.696)	(200)
4.95	30° 22′	2.94 (2.956)	(210)
6.25	36° 30′	2.46 (2.467)	(020)
7.10	40° 3′	2.25 (2.254)	(011)
7.40	41° 13′	2.19 (2.203)	(310)
7.60	41° 59′	2.15 (2.156)	(111)
7.95	43° 16′	2.09 (2.089)	(201)
9.20	47° 26′	1.92 (1.924)	(211)

[a] Wide-angle X-ray diffraction pattern (Laue method); Cu K_α radiation $\lambda = 1.5418$ Å; sample to film distance $L = 4.224$ cm.

[b] The values of the interplanar spacing d_{hkl} in brackets refer to the calculated values obtained from Ref. 9.

where α and β are the angles between the x-axis (the flow direction) and the crystallographic a- and b-axes, respectively. The c-axis orientation function f_c is obtained from the orthogonality relationship that exists among the three mutually perpendicular directions for an orthorhombic system. That is,

$$\overline{\cos^2\alpha} + \overline{\cos^2\beta} + \overline{\cos^2\epsilon} = 1 \tag{3}$$

and, therefore,

$$f_a + f_b + f_c = 0 \tag{4}$$

where ϵ is the angle between the x-axis (the flow direction) and the crystallographic c-axis. The crystalline orientation function is +1 for perfect orientation, zero for random orientation, and −0.5 for perpendicular orientation. A detailed account of the procedure for measurement of f_a and f_b from flat film photographs and the justification for the use of the form of eqs. (2a) and (2b) has been described previously.[27]

Table II shows the spacing of the (hkl) planes, which is representative of all samples investigated by the X-ray diffraction method. There were no differences between the microtomed samples analyzed. The reflections listed correspond to the region $15° < 2\theta < 55°$, where θ is the Bragg angle. The unit cell of the crystals is the ordinary orthorhombic type.[33]

Figures 5 and 6 show the variations of the orientation functions f for the crystallographic a-, b-, and c-axis in the depth direction at the location midway from the gate for the two resins molded at the melt temperature of 176°C. Figure 7 shows the variations of the crystallographic a-, b-, and c-axes in the depth direction at the corresponding location for resin EX2 molded at the high melt temperature of 205.9°C.

Generally, the a-axis tends to be oriented in the flow direction while the b- and c-axes vary symmetrically about this direction. Similar a-axis orientation has been observed in tubular blown films[34–36] and in the relaxation of stretched polyethylene films.[37–40] Furthermore, the variation of the orientations of the

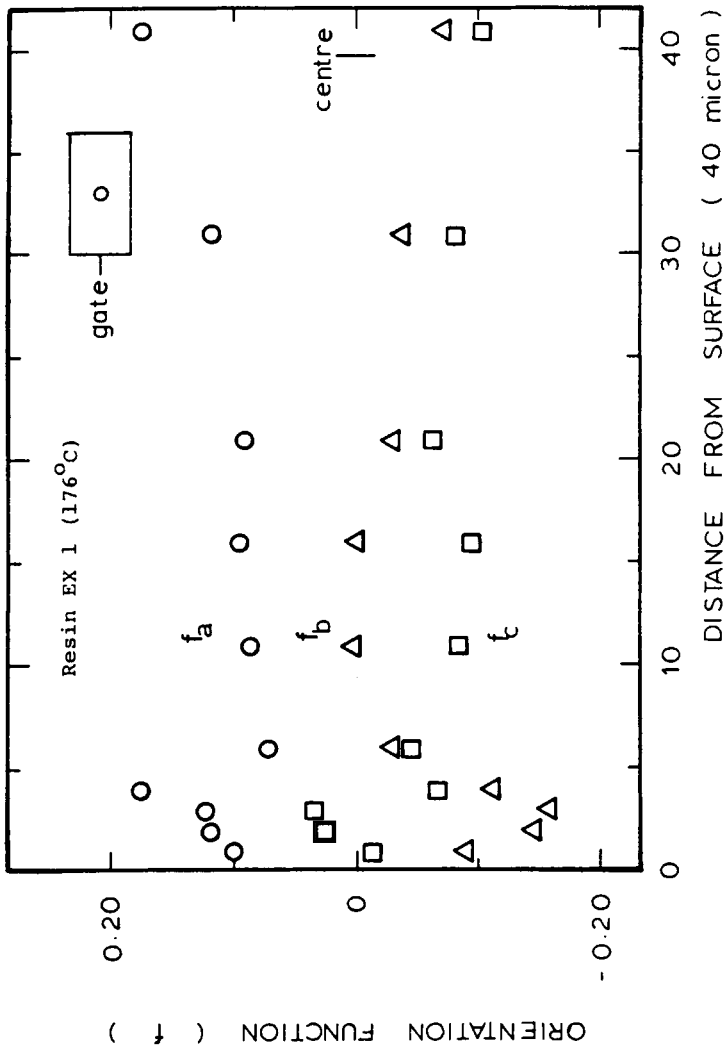

Fig. 5. Variation of the crystallographic axes in the depth direction.

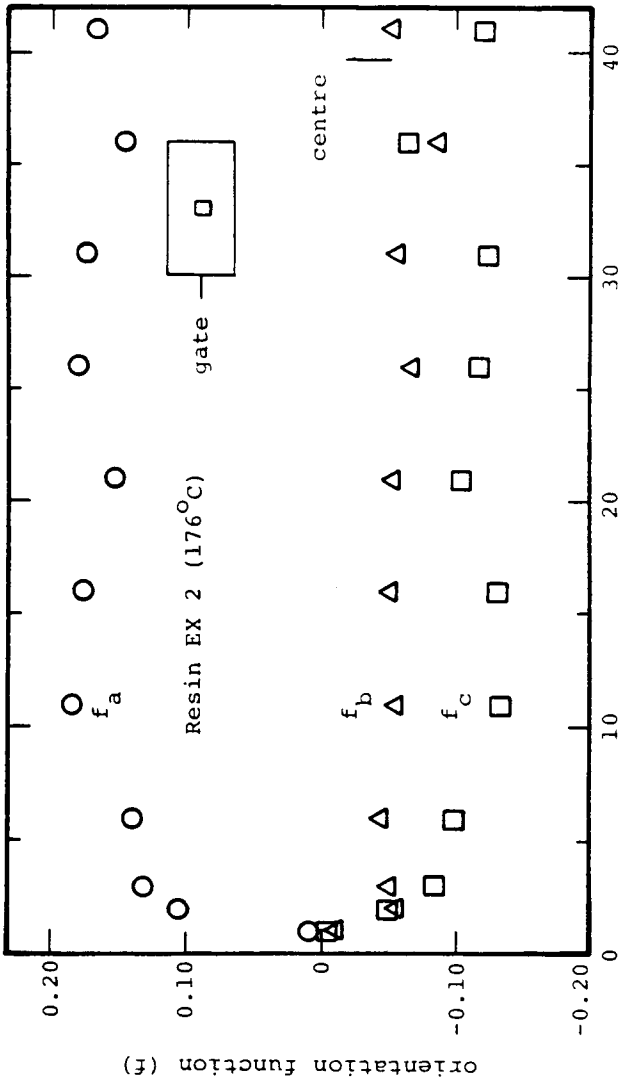

Fig. 6. Variation of the crystallographic axes in the depth direction.

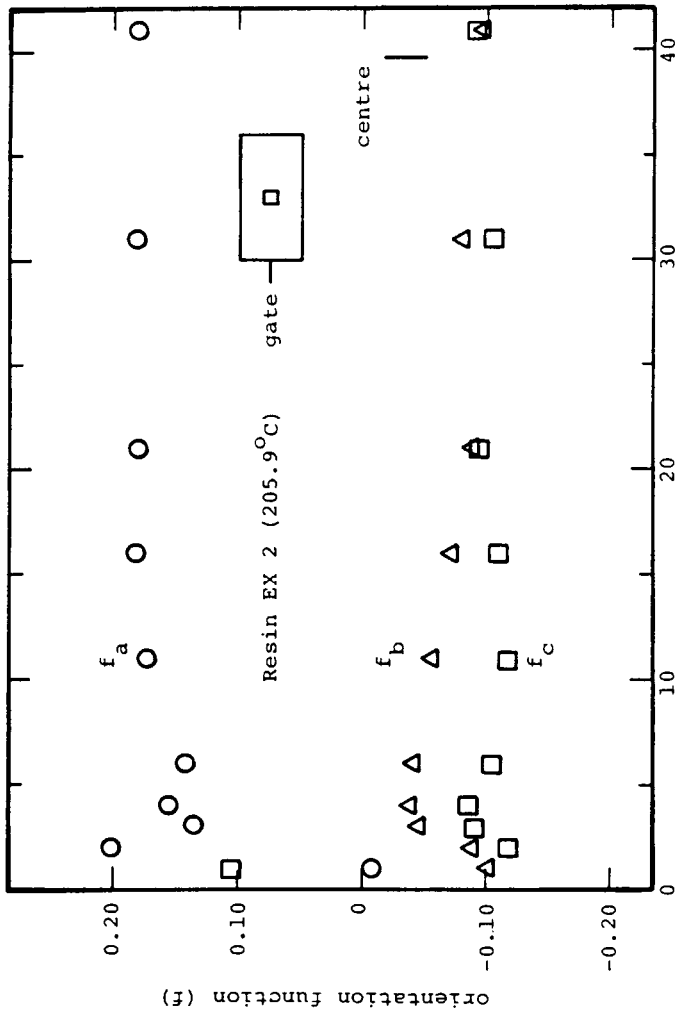

Fig. 7. Variation of the crystallographic axes in the depth direction.

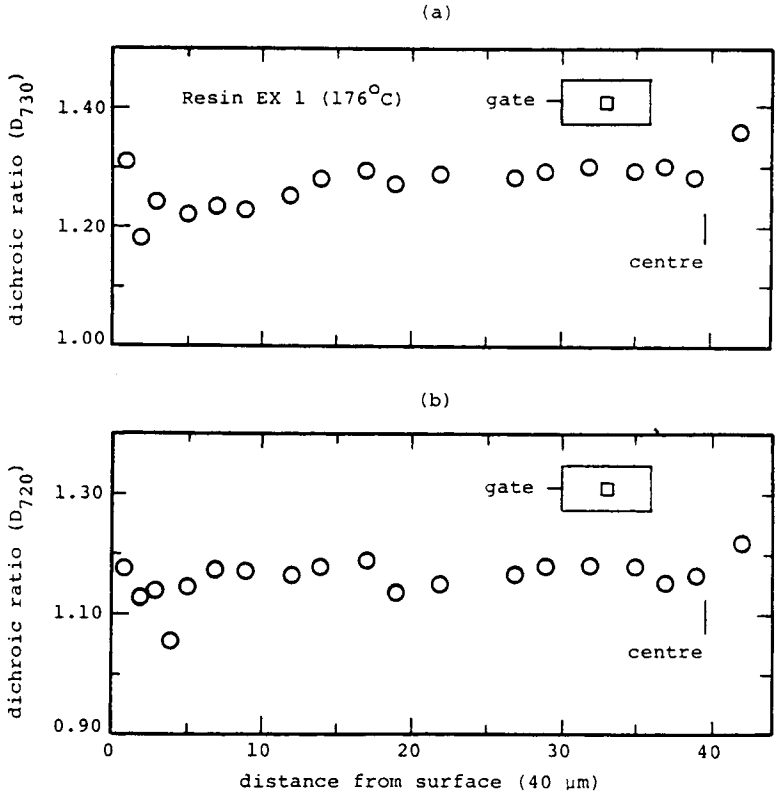

Fig. 8. Variation of dichroic ratio in the depth direction.

a-, *b*-, and *c*-axes tends to be most pronounced within the first 0.30 mm (300 μm) from the surface, beyond which the distributions remain constant.

The crystallite orientation, as represented by the orientation of the crystallographic axis in the flow direction, generally, tends to be maximum at or near the surface. This observation is consistent with the sonic modulus and birefringence measurements previously reported for these two resins molded under the same conditions.[22,27] Furthermore, Figure 5 shows that resin EX1, typically, tends to exhibit *a*-axis orientation throughout the molding, while Figures 6 and 7 show that resin EX2 tends to exhibit either relatively low *a*-axis orientation or high *c*-axis orientation in the skin layer and predominantly *a*-axis orientation towards the core of the molding.

The general increase in the degree of *a*-axis orientation as distance from the surface increases is attributed to the increase in the time for the molecular chains to relax due to the longer cooling times towards the core region of the molding. When the crystalline orientation distribution is compared at the corresponding locations, as shown in Figures 5 and 6, it is observed that resin EX1 tends to exhibit higher *a*-axis orientation near the surface (0–0.20 mm) than resin EX2. This is attributed to the fact that resin EX1 tends to crystallize later under shear and, therefore, experiences longer times for relaxation, which give rise to higher orientation of the *a*-axis.[37–40] The lower orientation of the *a*-axis towards the core is similarly due to the shorter times to relax than that experienced by resin EX2, since EX1 tends to crystallize sooner under pressure.[28,29] Furthermore,

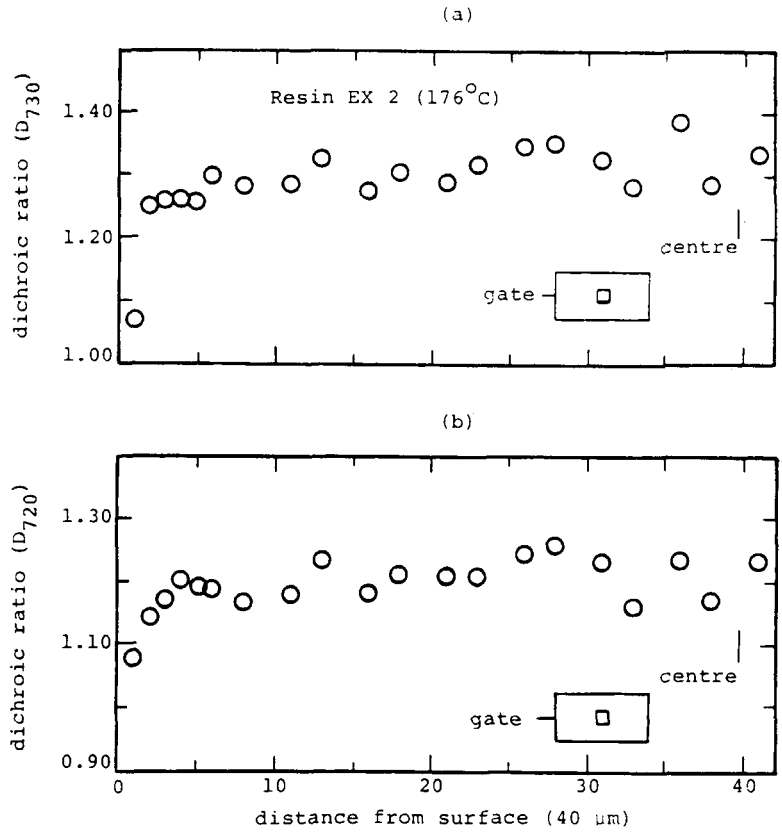

Fig. 9. Variation of dichroic ratio in the depth direction.

the observation that resin EX2 generally tends to exhibit either relatively low a-axis orientation or high c-axis orientation near the skin layer, as shown in Figures 6 and 7, is consistent with the shorter times to relax that resin EX2 experiences, since this resin tends to crystallize sooner under shear so that whatever orientation is induced during flow is retained.[28]

Generally, increasing the injection melt temperature tends to either increase the degree of a-axis orientation or decrease the degree of c-axis orientation away from the surface. The higher injection melt temperature leads to a longer time to relax and hence gives rise to either a relatively high degree of a-axis or a low degree of c-axis orientation away from the surface.[41–43] The explanation appears to be consistent with the results shown for resin EX2, as shown in Figures 6 and 7. Near the surface, the effects of cooling rates on crystallization rates and times to relax should be taken into consideration. These effects probably contribute to the complex behavior noted near the surface in Figures 6 and 7.

Infrared Measurements

The anisotropy parameter used in infrared studies is the infrared dichroic ratio, which is the significant factor in the interpretation of the optical anisotropy of the sample in terms of molecular orientation.

For an oriented polymer sample, the absorbance (A_L), measured with radiation

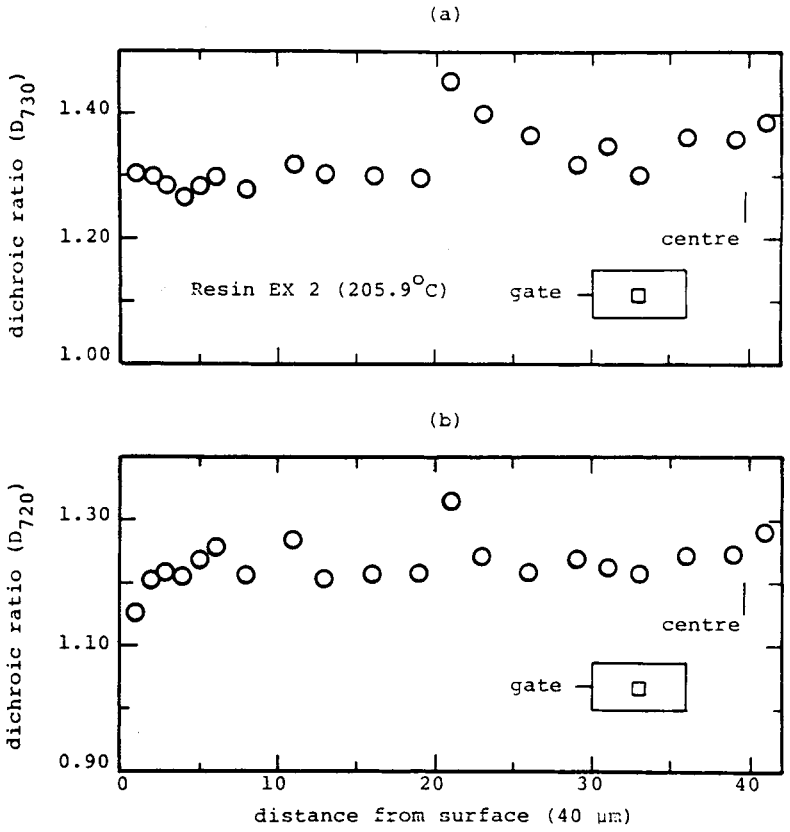

Fig. 10. Variation of dichroic ratio in the depth direction.

polarized in the stretched or flow direction may differ from the absorbance (A_T), determined for radiation polarized perpendicular to this direction. The dichroic ratio (D) is given by[44]

$$D = A_L/A_T = \epsilon_L/\epsilon_T \tag{5}$$

where ϵ is the absorbance per unit thickness of the deformed sample.

For partially crystalline polymers, infrared absorption peaks can arise form vibrations either within the crystalline phase or the amorphous phase or both.

Dichroic measurements on crystalline absorption peaks can be employed to study the orientation of certain crystallographic axes, providing that the direction of the transition moment with respect to the axes is known. In the polyethylene crystal, the well-known CH_2 rocking vibrations yields absorptions at about 720 cm^{-1} and 730 cm^{-1}, respectively. The 720 cm^{-1} band contains components due to both the crystalline and amorphous phases.[45]

In this study, the infrared band at 730 cm^{-1} is used to yield information concerning the crystalline orientation of the "a" crystallographic axis (f_a). By measuring the dichroic ratio of the 730 cm^{-1} band, the crystalline orientation of the a-axis is given by (45)

$$f_a = (D_{730} - 1)/(D_{730} + 2) \tag{6}$$

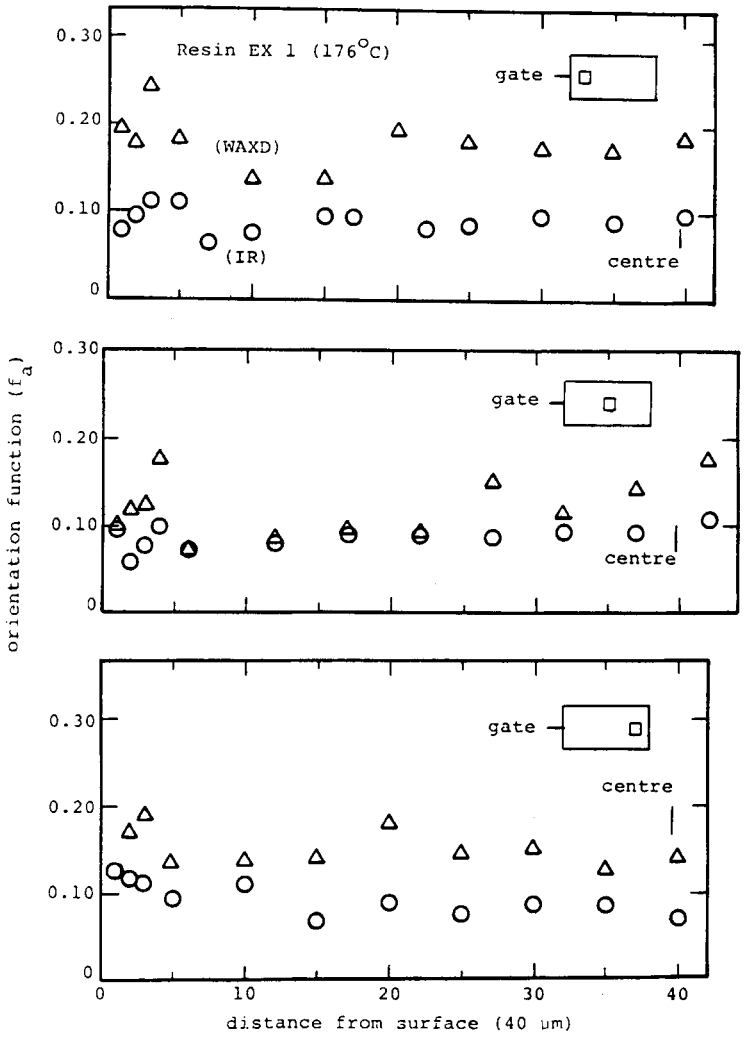

Fig. 11. Comparison of f_a obtained by X-ray diffraction and infrared dichroism.

where D_{730} is the measured dichroic ratio of the 730 cm^{-1} band.

Figures 8 and 9 show the alternate distributions of the dichroic ratios for both the 730 cm^{-1} and 720 cm^{-1} bands, respectively, for the location midway from the gate, for the two resins molded at a melt temperature of 176°C. Similarly, Figure 10 shows the alternate distributions of the two absorption bands at the corresponding location for resin EX2 molded at the high melt temperature of 205.9°C. A value of dichroic ratio lower than 1.0 signifies a preferred orientation in the longitudinal direction.

As shown in Figure 8, which pertains to resin EX1, the results of the dichroic ratio measurements for the CH_2 rocking vibration at the 720 cm^{-1} band absorption, which arises from both the crystalline b-axis and the amorphous phase, tend to exhibit a high value at the surface which decreases to a minimum near the surface and increases to a constant value towards the core. For resin EX2, as shown in Figures 9 and 10, generally, the dichroic ratio value obtained for the

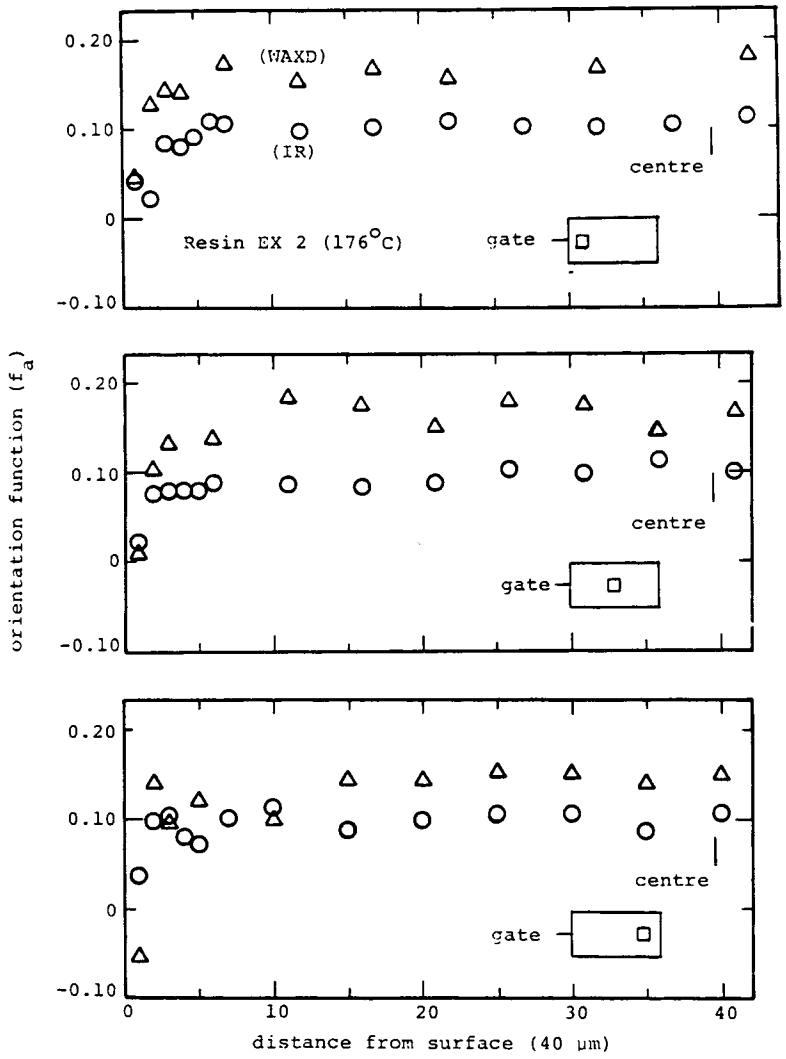

Fig. 12. Comparison of f_a obtained by X-ray diffraction and infrared dichroism.

720 cm^{-1} band absorption is observed to be relatively low at the surface, but increases to a maximum towards the core.

Generally, the crystalline a-axis absorption at the 730 cm^{-1} band tends to exhibit a minimum at or near the surface in all cases, as shown in Figures 8–10. This means that the degree of crystallite orientation tends to increase in the flow direction as distance from the surface increases. This observation appears to be consistent with the results of wide-angle X-ray diffraction measurements discussed earlier. Similar results of infrared measurements have been reported for polyethylene injection moldings.[46]

Comparison of the a-axis orientation distributions obtained by the X-ray diffraction technique and from measurement of the dichroic ratio pertaining to the 730 cm^{-1} absorption band are shown in Figures 11–13, at the various locations. The results show that the a-axis orientation distributions obtained by the two techniques appear to be in good agreement with each other. The two

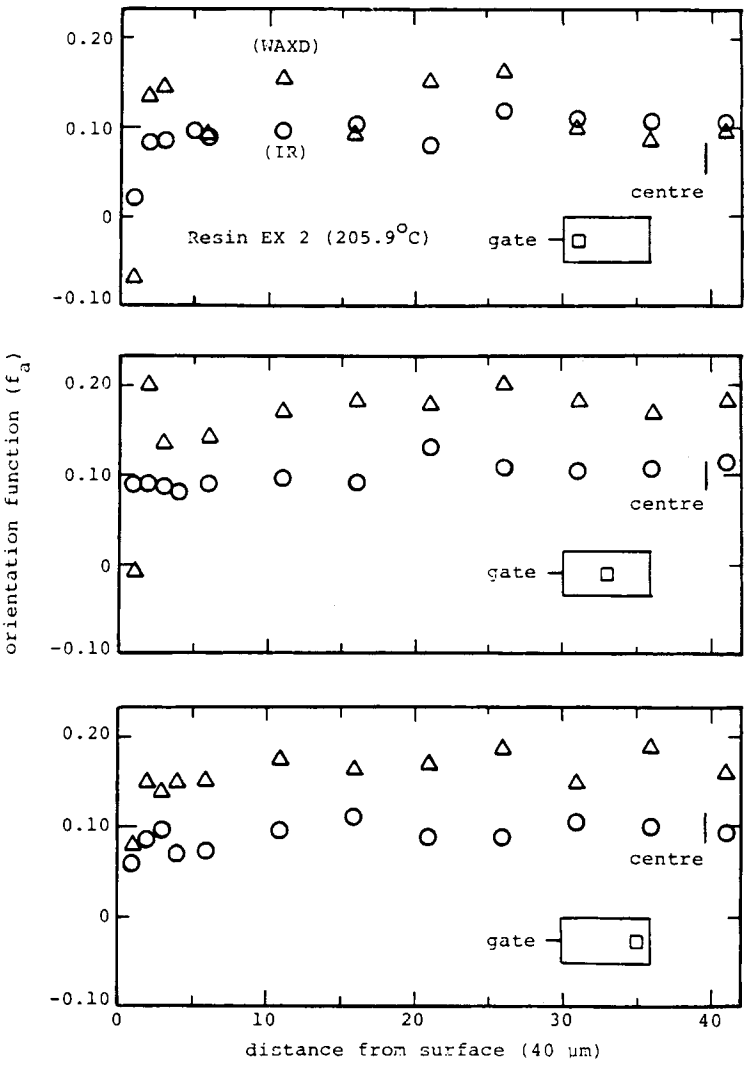

Fig. 13. Comparison of f_a obtained by X-ray diffraction and infrared dichroism.

techniques indicate that the a-axis is oriented in the flow direction and that the degree of orientation tends to increase as distance from the surface increases.

CONCLUSIONS

The techniques of density, X-ray diffraction, and infrared measurements have been employed with the aim of describing the distributions of crystallinity and orientation in injection molded parts. All techniques detect significant changes in crystallinity and orientation near the surface, which tend to disappear at a distance of approximately 200 μm (0.20 mm) from the surface. Other work carried out in our laboratory suggests that these differences have important ramifications on the ultimate performance, such as mechanical properties. In fact, it has been shown[23] that the distributions of optical and mechanical prop-

erties in the molding may be estimated with reasonable accuracy on the basis of a knowledge of the distributions of crystallinity and orientation functions.

Density measurements indicate that the degree of crystallinity (density) increases monotonically from the surface of the molding. The effect of higher injection temperature appears to be relatively small. However, it tends to raise the degree of crystallinity throughout the injection molded part.

X-ray diffraction results show that the crystallographic a-axis tends to be oriented in the flow direction. The a-axis distributions are consistent with those obtained by measurement of dichroic ratio pertaining to the 730 cm^{-1} absorption band. Maximum orientation is observed at or near the surface of the molding, and the distribution of orientation appears to be independent of the injection temperature. The two resins included in the study exhibited substantial differences in the distributions of crystallinity and orientation. These differences, in turn, are attributed to the complex interactions between resin properties and processing conditions during the molding cycle.

The authors wish to express their thanks to Mr. R. S. Pedersen and his colleagues from DuPont of Canada, Plastics Division, for supplying the materials included in this study and relevant information regarding these materials. Dr. Victor Tan and Dr. Dilhan Kalyon from McGill University were helpful in various aspects of the experimental and analytical work. Also, we would like to express our thanks for financial support from DuPont of Canada Ltd., the Natural Sciences and Engineering Research Council of Canada, the Ministère de l'Education of the Government of Quebec, and McGill University.

References

1. R. S. Spencer and G. D. Gilmore, *Mod. Plast.*, **28,** 97 (Dec. 1950).
2. D. H. Harvey and R. G. Parrot, *Polym. Eng. Sci.*, **10**(4), 209 (1970).
3. J. L. Berger and C. G. Gogos, *Polym. Eng. Sci.*, **13**(2), 107 (1973).
4. M. R. Kamal and S. Kenig, *Polym. Eng. Sci.*, **12**(4), 294 (1972).
5. M. R. Kamal and S. Kenig, *Polym. Eng. Sci.*, **12**(4), 302 (1972).
6. H. A. Lord and G. Williams, *Polym. Eng. Sci.*, **15,** 569 (1975).
7. P. Thienel and G. Menges, *Polym. Eng. Sci.*, **18,** 314 (1978).
8. E. Boehme, *Kunststoffe*, **60,** 273 (1970).
9. E. S. Clark, *Polym. Prepr.*, **14**(1), 268 (1973).
10. E. S. Clark and C. A. Garber, *Int. J. Polym. Mater.*, **1,** 31 (1974).
11. E. S. Clark, *Plast. Eng.*, 73 (March 1974).
12. M. R. Kantz, H. D. Newman, Jr., and F. H. Stigale, *J. Appl. Polym. Sci.*, **16,** 1249 (1972).
13. D. R. Fitchnun and Z. Menick, *J. Polym. Sci., Polym. Phys. Ed.*, **11,** 951, 973 (1973).
14. S. Y. Hobbs and C. F. Pratt, *J. Appl. Polym. Sci.*, **19,** 1701 (1975).
15. G. Menges and G. Wubken, *Soc. Plast. Eng. Tech. Pap.*, **19,** 519 (1973).
16. W. Woebiken and B. Heise, *Kunststoffe*, **68,** 99 (1978).
17. M. R. Kamal and V. Tan, *Polym. Eng. Sci.*, **19,** 558 (1979).
18. H. Keskkula and J. W. Norton, Jr., *J. Appl. Polym. Sci.*, **11,** 289 (1959).
19. M. Jensen and R. R. Whisson, *Polymer*, **14,** 193 (1973).
20. M. Fleissner, *Kunststoffe*, **63,** 597 (1973).
21. T. Fett, W. Nothdurft, and H. Racke, *Kunststoffe*, **63,** 168 (1973).
22. M. R. Kamal and F. H. Moy, *Soc. Plast. Eng. Techn. Pap.*, **26,** 316 (1980).
23. M. R. Kamal and F. H. Moy, *Chem. Eng. Commun.*, **12,** 253 (1981).
24. S. Kavesh and J. M. Schultz, *J. Polym. Sci., Part A-2*, **8,** 243 (1970).
25. V. Tan and M. R. Kamal, *Soc. Plast. Eng. Antec.*, **22,** 339 (1976).
26. Z. Bakerdjian and M. R. Kamal, *Polym. Eng. Sci.*, **17,** 96 (1977).
27. F. H. Moy and M. R. Kamal, *Polym. Eng. Sci.*, to appear.
28. D. Kalyon, "An Integrated Experimental Study of the Injection Molding Behavior of Polyethylene Resins," M. Eng. thesis, McGill University, Montreal, 1977.

29. M. R. Kamal, D. M. Kalyon, and J. M. Dealy, *Polym. Eng. Sci.*, to appear.
30. F. Kashani, "Studies About Thermal Conductivity and Thermal Diffusivity Measuring Apparatus," M. Eng. thesis, McGill University, Montreal, 1979.
31. R. S. Stein, *J. Polym. Sci.*, **31,** 327 (1958).
32. J. J. Hermans, P. H. Hermans, D. Vermass, and A. Werdinger, *Recl. Trav. Chim.*, **65,** 427 (1946).
33. M. Kakudo and N. Kasai, *X-ray Diffraction by Polymers*, Kodansha-Elsevier, New York, 1972, Chap. 11.
34. S. L. Aggarwal, G. P. Tilley, and O. J. Sweeting, *J. Appl. Polym. Sci.*, **1,** 91 (1959).
35. D. R. Holmes and R. P. Palmer, *J. Polym. Sci.*, **31,** 345 (1958).
36. P. H. Lindenmeyer and S. Lustig, *J. Appl. Polym. Sci.*, **9,** 227 (1965).
37. A. Brown, *J. Appl. Phys.*, **20,** 552 (1949).
38. R. A. Horsley and H. A. Nancarrow, *Br. J. Appl. Phys.*, **2,** 345 (1951).
39. D. R. Holmes, R. G. Miller, R. P. Palmer, and C. W. Bunn, *Nature*, **171,** 1104 (1953).
40. T. T. Li, R. J. Volungis, and R. S. Stein, *J. Polym. Sci.*, **20,** 199 (1956).
41. K. Kobayashi and T. Nagarawa, *J. Macromol. Sci. Phys.*, **B4,** 331 (1970).
42. V. Tan and C. G. Gogos, *Polym. Eng. Sci.*, **16,** 512 (1976).
43. V. Tan, private communication.
44. R. Zbinden, *Infra-red Spectroscopy of High Polymers*, Academic, New York, London, 1964.
45. B. E. Read and R. S. Stein, *Macromolecules*, **1**(2), 116 (1968).
46. V. Tan and M. R. Kamal, *J. Appl. Polym. Sci.*, **22,** 2341 (1978).

Received June 22, 1982
Accepted November 20, 1982
Corrected proofs received March 17, 1983